PLANT NANOMATERIAL JOURNAL

Review articles

B-SITE SUBSTITUTION EFFECTS (Fe, Mn, Ni) ON THE STRUCTURAL, ELECTRONIC, AND ELECTROCHEMICAL PROPERTIES OF $La_{0.7}Sr_{0.3}BO_3$ PEROVSKITES FOR INTERMEDIATE-TEMPERATURE SOFC CATHODES

Naya Andita, Tia Ayu Nafi Pratama, Abellia Dita Astiyasari,
Lovian Nadiva Nur Haur Latifah
Departement of Physics, Universitas Negeri Surabaya, 60231, Surabaya, Jawa Timur, Indonesia
*Correspondence: naya.23010@mhs.unesa.ac.id

ABSTRACT

The shift toward low-emission energy technologies is increasing interest in intermediate- temperature solid oxide fuel cells (IT-SOFCs), where cathode performance is crucial for system efficiency and durability. The perovskite compound $La_{0.7}Sr_{0.3}BO_3$ (B = Fe, Mn, Ni) is promising as a cathode material due to its flexible crystal structure and mixed ionic–electronic conductivity (MIEC) properties. This article comparatively reviews three main systems: $La_{0.7}Sr_{0.3}FeO_3$, $La_{0.7}Sr_{0.3}MnO_3$, and $La_{0.7}Sr_{0.3}NiO_3$ based on their crystal structure, metal ion valence, oxygen vacancy concentration, conductivity, oxygen reduction reaction (ORR) activity, and thermal and chemical stability. The analysis results indicate a trade-off between electrochemical activity and stability: the Fe system has high stability but moderate activity, the Mn system offers a balance of both, while the Ni system shows the highest activity but is susceptible to high-temperature degradation. Optimization of the composition and oxygen vacancy ($\delta \approx 0.10–0.18$) can improve the conductivity without compromising crystal stability. This study emphasizes the importance of composition engineering, surface modification, and composite cathode fabrication to produce more efficient and durable next-generation IT-SOFC perovskite cathodes.

Keywords: $La_{0.7}Sr_{0.3}BO_3$, perovskite, IT-SOFC, oxygen vacancies, cation valence, and thermal stability.

ISSN 3109-9939

INTRODUCTION

The global energy crisis and growing concerns about climate change are forcing the world to shift towards clean and sustainable energy sources. Since the 19th century, humans have relied on fossil fuels to generate electricity, which ultimately produces greenhouse gases such as CO_2, CH_4, and NO_x. These gases cause global warming and damage the environment [1]. Amidst this situation, the development of efficient and low-emission energy conversion technologies has become crucial [2 3]. One technology that has attracted attention is the Solid Oxide Fuel Cell (SOFC), as it is capable of converting the chemical energy of fuel directly into electrical energy. SOFCs are highly flexible because they can work with various types of fuel and their efficiency can reach 60–65% [4 5], while producing low pollution [6 7]. However, conventional SOFCs, which require high temperatures (>900 °C), face major problems, such as electrode assembly, temperature mismatch between components, and high production costs [8 9].

To address these issues, researchers turned to intermediate-temperature SOFC (IT-SOFC) technology, which operates at temperatures of 500–700°C [1]. Although its efficiency potential remains high, the impact of thermal degradation and material packaging issues can be better controlled [10 11]. The main factor affecting IT- SOFC performance is the cathode material. At intermediate temperatures, the mechanism of electron and ion transfer, as well as the activation of oxygen reduction reactions (ORR) on the surface, is more difficult to achieve using cathode materials commonly used for high temperatures. Therefore, a suitable cathode for IT-SOFC must have good electron and oxygen ion conductivity, be heat resistant, and be able to perform ORR reactions effectively [10 12].

One promising candidate for IT-SOFC cathodes is the perovskite oxide $La_{1-x}Sr_xBO_3$ (A = La/Sr; B = transition metal) [13 1] , due to its flexible crystal structure and combined ionic and electronic conductivity (MIEC) properties [10 11]. This property allows the transfer of electrons and oxygen ions to occur simultaneously in its crystal structure at intermediate temperatures [12 14]. Furthermore, research by Telford [15] shows that in the $La_{1-x}Sr_xFe_{1-y}Mn_yO_{3-\delta}$ system, the crystal structure and number of oxygen vacancies (δ) are influenced by the substitution of transition metals at the B site, thereby affecting the functional properties of the oxide. This combination makes La-based perovskite systems, particularly $La_{1-x}Sr_xBO_3$ (B = Fe, Mn, Ni), a strong candidate for IT-SOFC cathodes because they are able to maintain a balance between electrochemical activity and high-temperature stability. Previous studies have explored the $La_{1-x}Sr_xFeO_3$, $La_{1-x}Sr_xMnO_3$, and $La_{1-x}Sr_xNiO_3$ systems separately; however, the results are sometimes difficult to compare directly due to differences in the fabrication methods, test conditions, and characterization techniques used [16]. Cheraparambil et al. [17] studied the $LaNi_xFe_{1-x}O_3$ series using in-situ testing to determine the role of Ni and Fe in the formation of surface active sites, although this study focused on the Ni–Fe system without comparing the results with complete data for the Mn or pure Fe systems at the same $La_{0.7}Sr_{0.3}$ composition. Meanwhile, research on the manganite family ($La_{1-x}Sr_xMnO_3$) shows that variations in Sr content and the effects of high temperatures influence structure, magnetic properties, and local conductivity, although these studies are generally not designed to be directly compared with Ni or Fe-based series under the same synthesis and testing conditions [18]. Niu, Y. [12] emphasize that the decrease in ORR (oxygen reduction reaction) rate and cathode degradation are major obstacles for IT-SOFCs, so it is important to understand directly how substitution at site B (Fe, Mn, Ni) affects ORR kinetics, oxygen vacancy number, and thermal stability at the same base composition [10 19 20.]

Therefore, there is still an imbalance in understanding how the variation of transition metals at site B (Fe, Mn, Ni) affects the balance between electronic conductivity, oxidation-reduction reaction (ORR) activity, and thermal stability in the same $La_{0.7}Sr_{0.3}BO_3$ system. As a result, this article aims to conduct a systematic and comparative analysis of the impact of substitution at site B (Fe, Mn, Ni) on $La_{0.7}Sr_{0.3}BO_3$. The aspects analyzed include crystal structure and metal ion valence, oxygen vacancy concentration and ORR activity, electrical conductivity and magnetic properties, as well as thermal stability and suitability for IT-SOFC systems. By summarizing and critiquing the latest research results from the past five years, this article is expected to provide a comprehensive overview and direction for future research in designing efficient and durable perovskite cathodes for IT-SOFC applications.

1. La-based Perovskite Structure

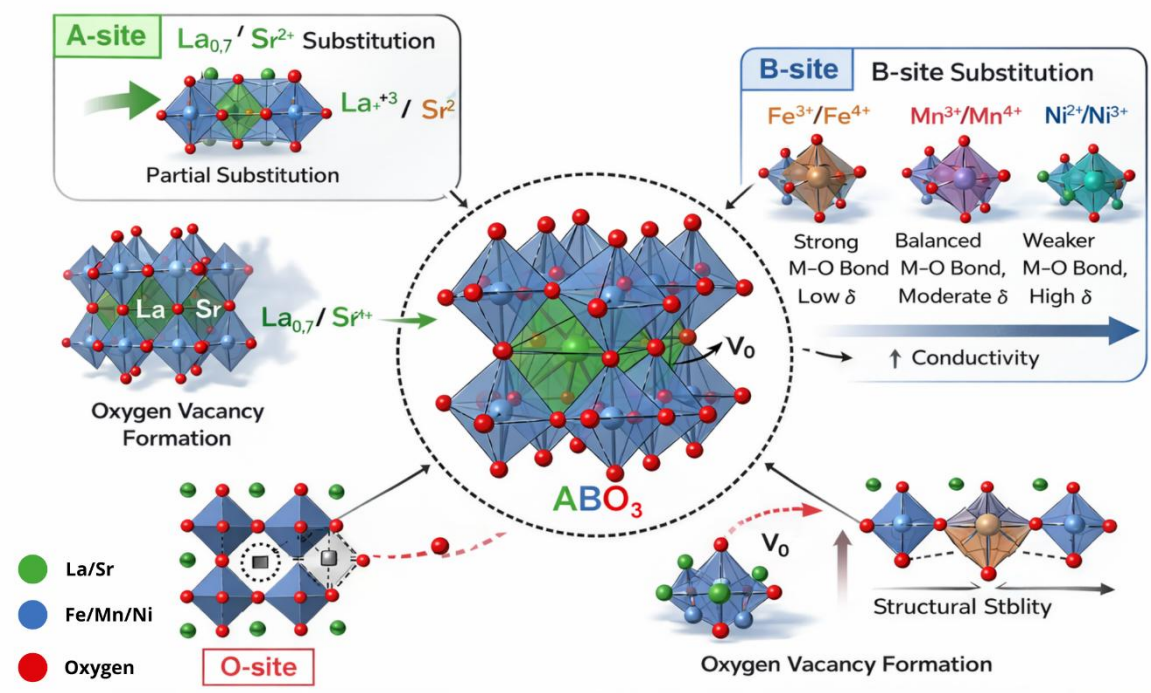

Figure 1. Schematic illustration of the ABO_3 perovskite structure highlighting A-site (La/Sr), B-site (Fe, Mn, Ni), and oxygen sublattices relevant to $La_{0.7}Sr_{0.3}BO_3$ cathodes.

Figure 1 illustrates the general ABO_3 perovskite framework relevant to $La_{0.7}Sr_{0.3}BO_3$ cathodes, highlighting the roles of the A-site, B-site, and oxygen sublattices. In this structure, La^{3+} and Sr^{2+} cations occupy the A-site positions, where partial substitution of La^{3+} by Sr^{2+} introduces charge imbalance that must be compensated within the lattice. This charge compensation occurs through changes in the oxidation state of the B-site transition metals and/or the formation of oxygen vacancies (V_O), a characteristic feature of non-stoichiometric perovskite oxides [21]. The B-site cations (Fe, Mn, or Ni) are located at the centers of BO_6 octahedra and play a dominant role in determining metal–oxygen bond strength, electronic transport behavior, and oxygen reduction reaction (ORR) activity. Oxygen anions coordinate the B-site cations and serve as the primary sites for vacancy formation, where the presence and distribution of oxygen vacancies significantly influence oxygen-ion diffusion and surface exchange kinetics [21 22]. As the B-site element varies from Fe to Mn and Ni, systematic changes in metal–oxygen bonding strength and oxygen vacancy concentration lead to a trade-off between structural stability and electrochemical activity, which underpins the performance of $La_{0.7}Sr_{0.3}BO_3$ cathodes in IT-SOFC applications.

Perovskites with an ABO_3 crystal structure, where A is a large cation and B is a transition cation such as Fe, Mn, or Ni, have a high ability to change their composition. By replacing ions in positions A and/or B, we can adjust the lattice structure, oxidation state, and number of oxygen vacancies (δ). In this system, the addition of Sr^{2+} or changing the type of ion in the B position with a different ion size will change the crystal shape from rhombohedral to cubic, along with an increase in the tolerance factor and the width of the B–O–B orbital band [13 14]. These changes have a direct impact on oxygen flow mechanisms and stability: more symmetrical (cubic) structures typically have better conductivity but weaker oxygen bonds, resulting in reduced oxidative stability [3 23].

The ionic and electronic conductivity (MIEC) properties of La-based perovskites arise due to variations in the charge levels of transition metal ions, which enable electron movement and oxygen ion diffusion through oxygen vacancies (δ). In the context of ion-tunnel solid oxide fuel cells (IT-SOFCs), the main challenge arises when the operating temperature is lowered to between 600 and 800 degrees Celsius, as the oxygen ion diffusion rate and oxygen reduction reaction (ORR) rate decrease significantly. Therefore, modification strategies at site B are crucial to maintain an optimal number of oxygen vacancies and enhance electronic conductivity at intermediate temperatures, in order to overcome the limitations of the ORR rate at IT [10 24 25]. Recent studies indicate that selective substitution at site B can alter the balance between electron mobility and oxygen stability; for example, increasing Ni content enhances conductivity but reduces the bond energy between metal and oxygen, while Mn tends to maintain a balance between thermal stability and ORR activity [17 26].

In general, $La_{0.7}Sr_{0.3}FeO_3$ has the best chemical and thermal stability in air, but its electron conductivity is relatively lower; $La_{0.7}Sr_{0.3}MnO_3$ exhibits a double exchange phenomenon that enhances ORR activity but with moderate conductivity while $La_{0.7}Sr_{0.3}NiO_3$ exhibits the highest conductivity and metallic properties, although it is more susceptible to oxygen loss at high temperatures [1 27]. Double-exchange redox is an electron transfer mechanism between mixed-valence cations such as Mn^{3+}/Mn^{4+} via Mn–O–Mn pathways, originally proposed by Zener, in which charge transport is intrinsically coupled with magnetic ordering [28 29]. These differences confirm that the interaction between B and O and the charge state of the transition metal are the main factors determining the performance of IT-SOFC cathodes. A summary of the structural and functional characteristics of the three systems is presented in **Table 1.** as a basis for analysis in the following section.

Table 1. Comparison of structural, electronic, and stability characteristics of $La_{0.7}Sr_{0.3}BO_3$ (B = Fe, Mn, Ni)

Parameter	Fe-based (LSF)	Mn-based (LSM)	Ni-based (LSN)
Crystal symmetry	Rhombohedral or pseudo-cubic structure stable under oxidizing conditions in air [23 30]	Orthorhombic/rhombohedral (composition & T_s dependent) [26 27 31]	Cubic [32]

Dominant valence state	Fe^{3+}/Fe^{4+} mixed valence confirmed by XPS/Mössbauer [33]	Mn^{3+}/Mn^{4+} double-exchange redox [26]	Ni^{3+}/Ni^{2+} mixed valence, strong 3d–2p hybridization [35 34]
Conduction mechanism	Small-polaron hopping between Fe^{3+}/Fe^{4+} sites [33]	Double-exchange Mn^{3+}–O–Mn^{4+} pathways [36]	Band-like conduction from delocalized Ni 3d–O 2p states [17 37]
Electrial conductivity at 700 °C	~10^2 S cm^{-1} [26 38]	10^2–10^3 S cm^{-1} [39]	10^3 S cm^{-1} at intermediate temperatures, high conductivity [17 32]
Oxygen vacancy (δ)	Low–moderate (0.05–0.10) [23]	Moderate (0.10–0.15) [39]	High (0.15–0.25) [34]
Magnetic ordering	Weak ferromagnetic coupling [15]	Strong ferromagnetic exchange, $T_(C)$ ≈ 350 °C [36]	Weak or paramagnetic [38 40]
ORR activity	Moderate (k^* ≈ 10^{-6}–10^{-5} cm s^{-1}) [41]	Moderate–good (especially nanostructured) [32 42]	Very high (k^* ≈ 10^{-4} cm s^{-1}, ASR ≈ 0.1 Ω cm^2 @ 700 °C) [17 43]
Thermal/chemical stability	High phase stability in air up to 900 °C under reported conditions [23 44]	Moderete, stable against YSZ and GDC [23 44]	Low, segregation and structural degradation reported under IT-SOFC conditions (≥ 700 °C) [45 46]

Based on the compiled literature, there is a trend that conductivity increases from Fe → Mn → Ni Based

on the compiled literature, there is a trend that conductivity increases from Fe → Mn → Ni under similar conditions [17 33 39] causing conductivity to increase with the expansion of d–p orbitals and bandwidth, as reported by Yamamoto et al. [23] and Pchelina et al. [26]. However, oxidative stability decreases due to the decrease in M–O bond energy and the increase in Ni–O orbital hybridization, which causes a tendency to lose oxygen at high temperatures[17 27]. This trend indicates a trade-off between ORR activity and thermal stability, which is the focus of further discussion in the section B-site Substitution Effects on Structural and Electronic Properties .

Based on the characterization results of the physical properties and electrochemical performance of these perovskite-based materials, a complex relationship is observed between chemical composition and the resulting material performance. The data indicates that changing the B-site composition from LSF to LSN significantly impacts electrical conductivity, oxygen defect formation, and catalytic ability in the oxygen reduction reaction (ORR) in distinct and contrasting ways (Figure 2).

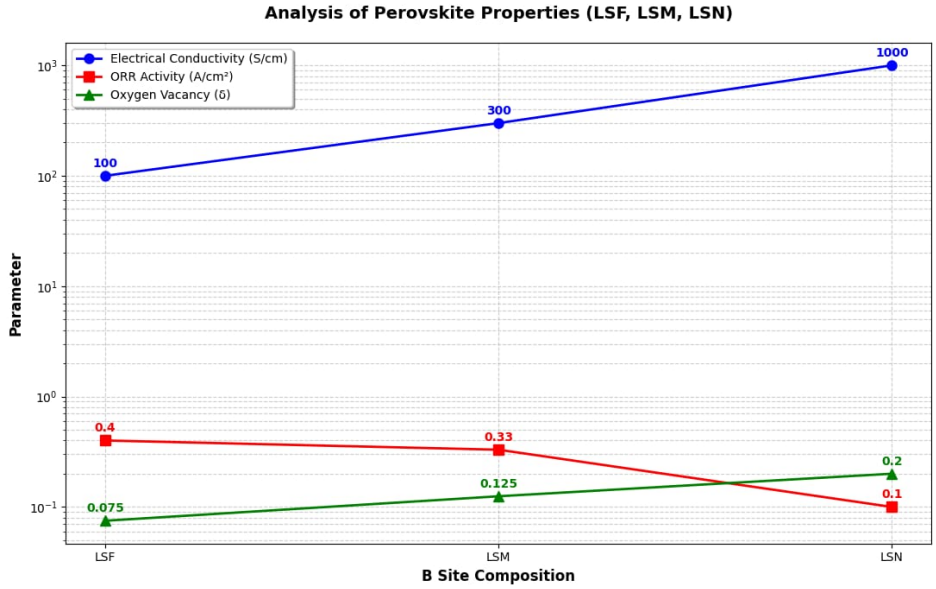

Figure 2. Comparison of electrical conductivity, oxygen vacancy (δ) and ORR activity of LSF, LSM, and LSN perovskite materials.

The electrical conductivity shows a highly significant upward trend as the B-site composition shifts from LSF to LSN. The LSF material exhibits a conductivity of 100 S/cm, which triples in LSM to 300 S/cm, and reaches its peak in LSN at 1000 S/cm. This sharp increase indicates that atomic substitution within the crystal structure, particularly in the LSN sample, successfully created a much more efficient electron transport pathway, making it the most superior material in terms of electrical conduction among the three samples.

In line with the conductivity trend, the oxygen vacancy concentration also experiences a consistent increase from LSF to LSN. LSF recorded the lowest oxygen vacancy level at 0.075 δ, which gradually increased in LSM 0.125 δ and reached the highest value in LSN 0.200 δ. This increase in oxygen defects suggests that the LSN structure possesses more vacant spaces within its crystal lattice, which theoretically could support higher oxygen ion mobility. This proves that the modification of the B-site composition directly influences the thermodynamic stability and defect formation of the material.

However, a contradictory result is observed in the ORR (Oxygen Reduction Reaction) activity, where performance actually declines as conductivity and oxygen vacancy increase. Despite having the lowest conductivity and oxygen vacancy, LSF exhibits the highest catalytic activity with a value of 0.40 A/cm². In

contrast, LSN, which excels in other physical properties, only recorded an ORR activity of 0.10 A/cm². This indicates that in this specific case, the oxygen reduction activity is more influenced by other factors, such as oxygen gas adsorption energy on the surface or more effective charge transfer mechanisms at the Iron (F) atoms, rather than relying solely on the high number of oxygen vacancies within the material.

2. Overview of Synthesis Routes and Their Influence on Perovskite Properties

Perovskites with the ABO_3 structure, including the $La_{0.7}Sr_{0.3}BO_3$ system (B = Fe, Mn, Ni), have been extensively synthesized using various routes, such as conventional solid-state reactions, sol–gel methods, the Pechini method, and sol–gel auto-combustion. The solid-state reaction method typically requires high calcination temperatures and prolonged heat treatment, which often leads to excessive grain growth and insufficiently homogeneous cation distribution. In contrast, wet-chemical approaches such as sol–gel and its derivatives enable cation mixing at the molecular level, resulting in improved compositional homogeneity and lower perovskite phase formation temperatures[46.]

Among these methods, sol–gel auto-combustion has been widely reported as an effective approach for synthesizing nanostructured perovskites. A study published in *RSC Advances* reported the successful synthesis of double perovskite Tb_2ZnMnO_6 via the sol–gel auto-combustion method, yielding nanosized particles with a well-defined perovskite crystal structure[47]. This result demonstrates that the self-sustaining combustion reaction can generate sufficient localized thermal energy to promote crystalline phase formation without requiring extremely high calcination temperatures, while simultaneously suppressing excessive grain growth. Similar findings have been reported for various other perovskite systems synthesized through sol–gel combustion routes, which consistently exhibit finer particle sizes compared to those produced by conventional solid-state reactions. Furthermore, a sol–gel–based review article published by MDPI emphasizes that molecular-level mixing enables better A-site and B-site cation homogeneity, reduces crystallization temperature, and provides more precise control over the morphology and stoichiometry of the final product[48]. These advantages are particularly important for $La_{0.7}Sr_{0.3}BO_3$ perovskites, as even minor variations in B-site cation distribution can significantly influence the crystal structure and functional properties of the material.

The synthesis method also plays a crucial role in determining oxygen vacancy formation and the functional properties of perovskites. A review on the role of oxygen vacancies in ABO_3 perovskite oxides indicates that catalytic activity toward the oxygen reduction reaction (ORR) is strongly correlated with the concentration and distribution of oxygen vacancies, which modify the electronic structure, crystal lattice, and surface chemistry of the material[21]. These oxygen vacancies are influenced not only by chemical composition but also by synthesis conditions, including sol–gel combustion methods, which tend to induce higher oxygen nonstoichiometry due to the combustion process and intermediate-temperature calcination [49].

3. B-site Substitution Effects

Variations in electrochemical behavior among $La_{0.7}Sr_{0.3}BO_3$ perovskites (B = Fe, Mn, Ni) originate from differences in B-site chemistry, which directly governs metal–oxygen bond strength and defect formation within the lattice. Substitution at the B-site modifies the electronic structure of transition-metal cations and regulates oxygen vacancy concentration (δ), thereby controlling mixed ionic–electronic conductivity and oxygen reduction reaction (ORR) kinetics in perovskite cathodes[21,49liu]. It has been widely reported that oxygen vacancy concentration acts as a key descriptor for ORR activity in ABO_3-type perovskite oxides, as vacancies facilitate oxygen adsorption, dissociation, and ion transport at the cathode surface[50,25]. In Fe-based perovskites, strong metal–oxygen bonding suppresses oxygen vacancy formation,

resulting in high structural stability but limited ionic transport and moderate ORR activity. In contrast, Ni-containing perovskites exhibit weaker metal–oxygen bonding and higher covalency, which promote increased oxygen vacancy concentrations and enhanced electronic conductivity, leading to superior ORR kinetics but reduced chemical stability under operating conditions. Mn-based systems occupy an intermediate regime, where reversible Mn^{3+}/Mn^{4+} redox chemistry enables balanced oxygen vacancy formation and mixed conduction while maintaining acceptable durability. These trends demonstrate that conductivity, oxygen vacancy concentration, and ORR activity in $La_{0.7}Sr_{0.3}BO_3$ cathodes are intrinsically coupled through B-site–controlled defect chemistry and must be interpreted as interdependent parameters rather than independent metrics.

3.1. Fe-based System: $La_{0.7}Sr_{0.3}FeO_3$

3.1.1. Structure and Electronic Properties

The iron-based perovskite $La_{0.7}Sr_{0.3}FeO_{3-\delta}$ (LSF) exhibits a rhombohedral or pseudo-cubic structure that remains stable under oxidizing environments up to approximately 900 °C [23]. Partial substitution of La^{3+} with Sr^{2+} generates mixed-valence Fe^{3+}/Fe^{4+} states, contributing to the formation of p-type charge carriers and enabling mixed ionic– electronic conductivity (MIEC). This dual-conduction mechanism arises from small-polaron hopping facilitated by the Fe–O–Fe network, where localized charge transfer occurs between Fe^{3+} and Fe^{4+} ions [51 52]. Recent studies further indicate that higher Sr content improves the ordering of FeO_6 octahedra, thereby reducing lattice distortion. Additionally, advanced XPS analyses report that the surface Fe^{4+} fraction increases at higher Sr compositions, enhancing charge carrier mobility [53]. X-ray diffraction investigations reveal a slight contraction in lattice parameters with increasing Sr content, while XPS and Mössbauer studies show that a stable 35–40% Fe^{4+} fraction is maintained—crucial for sustaining high electronic mobility without inducing structural distortion. DFT-based calculations also show that stabilization of Fe^{4+} eg orbitals plays a key role in preserving mixed-conducting behavior at intermediate operating temperatures [54]. These findings are reinforced by Mössbauer results confirming the strong bonding character of Fe–O under oxidative environments [55]. The resulting structure maintains robust Fe–O bonding, ensuring chemical stability in air..

3.1.2. ORR Activity

The oxygen reduction reaction (ORR) activity of LSF originates from its ability to transport both oxygen ions and electronic holes across the cathode interface. However, according to [56 57], the surface exchange coefficient (k) of LSF is lower than that of Mn- or Ni-based LSF owing to its limited oxygen vacancy formation. Surface-sensitive spectroscopic analyses further indicate that the concentration of oxygen-containing surface species increases only slightly with Sr doping. These results agree with findings that surface-site activation in LSF is hindered by its relatively high vacancy formation energy [58]. This suggests that further activation strategies—such as Co or Ni co-doping—are essential to enhance surface oxygen mobility [11 59] demonstrated that transition-metal co-doping can reduce O_2 adsorption energy and improve ORR kinetics. Surface reconstruction treatments through redox cycling have also been shown to enhance oxygen mobility and diffusivity [60]. Nevertheless, LSF maintains acceptable ORR activity combined with strong durability, making Fe-based cathodes attractive for long-term IT-SOFC operation—especially in systems where dimensional and structural stability are prioritized over peak performance [61]. This observation is further supported by results from Ni-doped Fe-based perovskites, which demonstrate efficient and stable long-term cathodic performance under IT-SOFC conditions [62] .

3.1.3. Electrical and Magnetic Conductivity

Electrical conduction in LSF is primarily governed by small-polaron hopping, especially the localized holes on Fe^{4+} ions, which yield typical conductivities of ~10^2 S cm^{-1} at 700 °C [63]. In this research, electrical conduction in La–Fe perovskites was examined using impedance spectroscopy, and the results confirm that conduction occurs via polaron-hopping mechanisms—supporting claims that small polarons dominate charge transport in Fe-based perovskites [64]. Computational and experimental studies have also shown how oxygen vacancies and structural defects influence hole mobility and electrical conductivity in La– Sr–Fe compositions [65] [63]. These electron-transport processes are closely linked to the magnetic ordering through Fe^{3+}–O– Fe^{4+} double-exchange interactions; the relationship between Fe valence states, Fe–O bonding, and electron exchange pathways has been analyzed both theoretically and experimentally [66]. Furthermore, B-site modifications are known to alter oxidation states and vacancy concentrations, thereby affecting both conductivity and magnetic/electrochemical performance in Fe-based perovskites, as reported in modified LSF systems [67]. As temperature increases, long-range ferromagnetic order diminishes; however, short-range spin correlations persist, enhancing charge mobility under IT conditions—consistent with thermally activated polaron hopping models and defect-influenced transport [65] [66]. This spin-assisted transport also explains the weak magnetoresistive behavior commonly observed in Fe-based perovskites. Unlike Ni-based perovskites, whose conduction is more band-like and lacks significant magnetic contributions, Fe-based materials retain magnetically mediated conductivity that stabilizes electronic pathways against lattice variations [63] [67].

3.1.4. Thermal Stability and Suitability for IT-SOFC

$La_{0.7}Sr_{0.3}FeO_{3-\delta}$ is well known for its excellent thermal and chemical stability under oxidizing atmospheres across intermediate–high temperatures. Recent studies show that LSF retains its perovskite structure without major decomposition during repeated heating cycles or long-term operation [67] [68]. B-site compositional modifications—such as Pt, Ru, or low-electronegativity metal substitution—have also been shown to enhance oxidation resistance and structural stability, partly through Fe valence redistribution and oxygen vacancy regulation [69]. Moreover, studies on transition-metal-doped Fe-based perovskites reveal improved redox tolerance and mechanical strength under IT-SOFC conditions, while maintaining good thermal compatibility with common electrolytes such as GDC. Therefore, although Fe-based perovskites may not deliver the highest ORR activity compared with Co-based materials, their combination of phase stability, chemical robustness, and thermal compatibility makes them strong candidates for IT-SOFC cathodes—either as standalone materials or as components within composite architectures [70].

3.2. Mn-based System: $La_{0.7}Sr_{0.3}MnO_3$

3.2.1. Structure and Electronic Properties

The manganese-based perovskite $La_{0.7}Sr_{0.3}MnO_3$ (commonly referred to as LSM) typically forms either a rhombohedral or orthorhombic crystalline structure, influenced by the concentration of Sr and the temperature during synthesis [71]. When La^{3+} is partially replaced by Sr^{2+}, it creates mixed valence states of Mn^{3+} and Mn^{4+}, which enhances conductivity through double-exchange mechanisms along Mn^{3+}–O–Mn^{4+} links. An increase in Sr concentration results in a slight reduction of lattice distortion due to the smaller ionic radius of Mn^{4+}, which improves the overlap of Mn–O–Mn and stabilizes the movement of charge carriers [72]. Investigations using XPS and XANES demonstrate that the ratio of Mn^{3+} to Mn^{4+} is highly influenced by the partial pressure of oxygen, which has a direct impact on electronic conductivity and the development of oxygen vacancies. The perovskite structure maintains its

stability at temperatures up to roughly 900 °C in air, with limited occurrence of phase segregation or decomposition [73].

3.2.2. ORR Activity

Among the lanthanum-based perovskites, LSM is well-known for its excellent stability, although it has relatively limited oxygen-reduction activity [74]. The step that limits the rate of the oxygen reduction reaction (ORR) in LSM is the exchange of surface oxygen, which is obstructed by the low levels of mobile oxygen vacancies (δ < 0.1). Nonetheless, various studies indicate that nano-structured LSM or compositions with a deficiency in A-site cations ($La_{0.65}Sr_{0.3}MnO_{3-\delta}$) can greatly improve ORR activity by enhancing the density of surface defects. Additionally, manganese exhibits strong redox reversibility ($Mn^{3+} \leftrightarrow Mn^{4+}$), which contributes to the retention of catalytic stability during cycling. The implementation of composite cathodes, such as mixtures of LSM–GDC or LSM–LSGM, has been effective in enlarging the active surface area and enhancing the transport of oxygen ions [75]. Although LSM has lower intrinsic activity compared to nickel-based systems, its steady-state performance is still sufficient for prolonged operation in intermediate temperature solid oxide fuel cell (IT-SOFC) settings [76].

3.2.3. Electrical and Magnetic Conductivity

The electronic conduction mechanism in LSM is chiefly influenced by the double-exchange interactions among Mn^{3+} and Mn^{4+} ions, which are closely linked to the local spin ordering [77]. As the temperature rises from 300 to 800 °C, the material changes from a ferromagnetic to a paramagnetic state, coinciding with a gradual reduction in conductivity caused by spin disorder. Nevertheless, even beyond the Curie temperature (approximately 350 °C), the process of small-polaron hopping maintains moderate conductivity levels (10^2–10^3 S cm^{-1} at 700 °C) [78]. In comparison to Fe-based counterparts, LSM exhibits superior magnetic conductivity and a more significant magnetoresistive response due to enhanced spin coupling. The Mn–O–Mn exchange shows high sensitivity to the oxygen stoichiometry δ; when δ exceeds 0.15, the magnetic order diminishes, leading to a notable fall in conductivity [79]. Nonetheless, the magnetic aspect of charge transport positively influences electronic stability during extended operation.

3.2.4. Thermal Stability and Suitability for IT-SOFC

Thermochemical stability is a significant benefit of cathodes made from LSM. This material shows very low reactivity with widely used electrolytes, including YSZ, CGO, and LSGM, and maintains its structural integrity even after extended exposure to temperatures of 800 °C [80]. Thermogravimetric studies indicate minimal weight loss up to 950 °C, demonstrating strong resistance against reduction and oxygen loss. Nevertheless, the moderate range of δ that supports magnetic conduction also restricts the transport of oxygen, resulting in moderate rates of the oxygen reduction reaction (ORR) and greater area-specific resistance (ASR) in comparison to nickel-based alternatives. Regardless, the favorable combination of solid phase stability, moderate electrical conductivity, and exceptional redox tolerance renders LSM a compelling choice for cathodes in intermediate temperature solid oxide fuel cells (IT-SOFCs), especially in scenarios where reliability is more crucial than achieving the highest power output [81].

3.3. Ni-based System: $La_{0.7}Sr_{0.3}NiO_3$

3.3.1. Structure and Electronic Properties

Recent studies have shown that $LaNiO_3$ (LNO) retains a rhombohedral perovskite structure (space group $R\bar{3}c$), which originates from the rotation and tilting of the NiO_6 octahedra. These

structural distortions can be further modified by epitaxial strain in thin-film growth, where lattice parameters and the Ni–O–Ni bond angle change depending on the substrate, thereby influencing the orbital distribution of Ni-3d electrons and their hybridization with oxygen[82]. As a result, LNO exhibits metallic behavior: the Ni^{3+} electronic configuration (d^7, with fully filled t_2g and a partially filled e_g orbital) produces highly delocalized e_g states due to strong Ni-3d–O-2p hybridization, which explains the high electrical conductivity observed in both bulk and thin-film samples compared to other 3d-transition-metal perovskites[83].

Moreover, structural modifications such as epitaxial strain, oxygen vacancies, and reduced dimensionality have been shown to strongly influence this electronic behavior. For instance, resistivity variations in strained LNO thin films indicate that tensile strain can induce higher resistivity due to modified oxygen stoichiometry and partial reduction of Ni^{3+} to Ni^{2+}, which disrupts the conduction pathway[84]. At the atomic scale, oxygen-vacancy formation and surface reconstruction can further alter the charge distribution and density of states near the Fermi level, affecting stability and electronic mobility under operational conditions[85].

3.3.2. ORR Activity

Ni-containing perovskite oxides have emerged as promising non-precious electrocatalysts for the oxygen reduction reaction (ORR) due to their tunable surface chemistry, flexible electronic structure, and ability to host oxygen vacancies that enhance oxygen adsorption and activation. Recent studies demonstrate that combining Ni with other transition metals (or introducing Ni into Co/Fe perovskite frameworks) can optimize the eg orbital occupancy and Ni-3d/O-2p hybridization, two key descriptors correlated with ORR activity—leading to improved onset potentials and higher limiting currents compared to undoped oxides[86,87]. In addition, engineering of the perovskite surface (e.g., creating cation deficiencies or controlled oxygen vacancies) increases the number of active sites and facilitates O–O bond cleavage via a lattice-oxygen mediated mechanism, which significantly enhances ORR kinetics in alkaline media[88]. Practical implementations also show that integrating Ni-based perovskites with conductive supports or producing nanocomposite architectures (perovskite + carbon/MWNTs) improves mass transport and electronic conductivity, producing ORR performances that approach those of Pt-based catalysts in specific device tests such as Zn–air and microbial fuel cells[89.]

In addition to B-site compositional modification, surface engineering through Ni exsolution (the formation of partially “socketed” Ni nanoparticles emerging from the perovskite matrix) and the introduction of nanoporosity have been shown to increase the number of surface active sites and enhance catalytic stability. Experimental reports demonstrate that nanoporous materials with exsolved particles exhibit significantly higher ORR/OER activity and better cyclic stability than conventionally sintered materials. These effects are attributed to the combination of improved surface conductivity, strong metal–oxide interactions enabled by socketing, and favorable particle-size distributions for O–O bond dissociation[90,91].

3.3.3. Electrical and Magnetic Conductivity

Ni-based perovskite oxides exhibit strong potential as high-conductivity materials, where the electrical transport properties are largely influenced by B-site Ni substitution, oxygen non-stoichiometry, and mixed-valence electronic configurations. Recent studies on $PrNi_{0.4}Fe_{0.6}O_{3-\delta}$ and $PrNi_{0.4}Co_{0.6}O_{3-\delta}$ demonstrate that incorporation of Ni significantly enhances charge transport due to increased carrier concentration and improved overlapping

between Ni-3d and O-2p orbitals, resulting in improved electron mobility and band delocalization relative to undoped perovskites[92]. This enhancement arises from the formation of mixed valence states (Ni^{2+}/Ni^{3+}) and the presence of oxygen vacancies, which support electron hopping mechanisms and stabilize conduction pathways beneficial for intermediate-temperature electrochemical operation[92]. In addition, compositional engineering strategies utilizing Ni-based co-doping have demonstrated that Ni can effectively tune electronic density near the Fermi level, thereby increasing conductivity while simultaneously improving electrocatalytic performance, indicating its dual functional benefit in perovskite frameworks (She et al., 2022). Further, Fe/Ni co-doped perovskites such as $BaCo_{0.6}Fe_{0.2}Ni_{0.2}O_{3-\delta}$ exhibit enhanced electronic conductivity due to cooperative oxygen defect chemistry and stronger B–O hybridization, confirming that Ni plays a critical role in facilitating rapid charge transfer within the crystal lattice[93]. Overall, these results confirm that Ni incorporation systematically improves electrical conductivity through oxygen-vacancy engineering, mixed-valence charge transfer, and orbital hybridization optimization—making Ni-based perovskites strong candidates for high-performance electrodes in SOFCs, PCFCs, and other electrochemical energy conversion devices.

3.3.4. Thermal Stability and Suitability for IT-SOFC

Ni-doped and Ni-containing perovskite oxides can maintain structural integrity and functional performance under elevated temperatures if properly engineered. For instance, a comprehensive review on Ni-perovskite-based catalysts demonstrated that when synthesized at high temperatures, Ni-containing perovskite oxides exhibit thermal stability comparable to conventional supported metal catalysts, suggesting that Ni substitution does not necessarily compromise high-temperature operability[94]. In another important study, exsolved Ni nanoparticles on a perovskite oxide matrix (e.g. acceptor-doped $SrTi_{0.95}Ni_{0.05}O_{3-\delta}$, or donor-type variants) were investigated: the authors found that the thermal stability of exsolved Ni particles depends strongly on the defect chemistry of the parent perovskite — specifically, oxygen vacancy concentration and surface defect characteristics, where donor-type doping yielded more stable nanoparticle dispersion under thermal treatment than acceptor-type doping[95]. This indicates that, with proper B-site doping and defect engineering, Ni-based perovskites can sustain high-temperature conditions without rapid degradation or particle agglomeration. More broadly, advances in nanostructured perovskite oxides indicate improved thermal and structural robustness, making them viable for electrocatalysis and energy-conversion applications[96]. Moreover, in the context of perovskite solar cells (PSCs), even though organic–inorganic halide perovskites face severe thermal instability, the trend toward fully inorganic perovskite oxides (including Ni-based metal oxides) reflects their superior thermal endurance and potential for long-term operation under heat stress[97]. In-situ analyses and coarsening studies show that the stability of exsolved Ni particles strongly depends on the defect chemistry of the host perovskite and on the applied thermal-treatment conditions[98]. Perovskites with a balanced oxygen-vacancy concentration and appropriate donor/acceptor doping are able to suppress particle coalescence more effectively, thereby maintaining a fine nanoparticle distribution over prolonged operating temperatures. Therefore, beyond synthesis parameters alone, design strategies that target vacancy control and A-/B-site stoichiometry can significantly enhance the thermal durability of Ni-exsolved electrocatalysts in IT-SOFC systems[99].

.

4. Comparative of B-site Substitution Effects

To reinforce the findings presented previously, Table 1 provides an overview of the essential physicochemical and electrochemical properties of $La_{0.7}Sr_{0.3}BO_3$ (B = Fe, Mn, Ni) materials. The introduction of different transition-metal cations results in unique changes in lattice structure, oxygen ratios, and electronic configuration, which ultimately influence their viability as cathodes in intermediate-temperature solid oxide fuel cells (IT-SOFCs).

Fe-based perovskites are characterized by their remarkable structural and thermal resilience, but they exhibit limited electronic and ionic transport capabilities due to the relatively confined hopping of Fe^{3+}/Fe^{4+} ions. In contrast, Mn-based systems, which rely on the Mn^{3+}/Mn^{4+} double exchange mechanism, offer moderate conductivity and enhanced magnetic interactions, resulting in satisfactory oxygen reduction reaction (ORR) performance along with good redox reversibility. Conversely, Ni-based systems stand out for their superior electronic conductivity and surface oxygen mobility, attributed to the extensive overlap of Ni–O orbitals. Nevertheless, these benefits are accompanied by challenges regarding chemical durability, as the bonding between Ni–O becomes weaker and the formation of oxygen vacancies accelerates degradation [21 47].

5. Correlative between Oxygen Vacancy, Valance, and ORR Activity

An integrated comparative and correlative discussion of $La_{0.7}Sr_{0.3}BO_3$ (B = Fe, Mn, Ni) perovskite systems is presented in this section, with an emphasis on the effects of B-site substitution on the structural, electronic, and electrochemical properties that are pertinent to IT-SOFCs. To create systematic correlations between lattice distortion, oxygen nonstoichiometry (δ), valence state, conductivity, oxygen reduction reaction (ORR) activity, and long-term stability, the analysis synthesizes data.

B-site replacement significantly changes the crystal symmetry and electrical structure of $La_{0.7}Sr_{0.3}BO_3$ perovskites. Yamamoto et al. [23] and Sánchez-Caballero et al. [30] found that Fe-based compositions often have rhombohedral or pseudo-cubic symmetry and stable Fe^{3+}/Fe^{4+} redox couples. Mn substitution improves Mn^{3+}/Mn^{4+} double-exchange conduction by shifting the structure to orthorhombic symmetry [26 100]. Ni substitution brings the lattice closer to its ideal cubic form, improving the tolerance factor and orbital overlap [27 40]. Spectroscopic experiments (XPS/XANES) reveal that Ni-based perovskites have higher covalency and lower M-O bond strength [17 101]. Co-doped systems (e.g., $La_{0.7}Sr_{0.3}Fe_{0.5}Ni_{0.5}O_3$) have intermediate structural distortions and enhanced electrical channels [102].

By expanding the bandwidth and promoting mixed ionic-electronic conduction (MIEC), the substitution of Fe by Mn and Ni drastically increases electronic conductivity. At 700°C, Fe-based systems typically exhibit a conductivity of ~10^2 S cm^{-1} [33], Mn-based systems range from 10^2 to 10^3 S cm^{-1} [3 103 104]. Perovskites made from Ni, particularly La_0. Senior. Due to its greater carrier mobility, $_3NiO_3-\delta$ can exceed 10^3 S cm^{-1} [9 17]. Microstructural optimization, including controlled sintering [105] and surface reconstruction [37] further enhances ORR activity [21]. Shaheen et al. [42] emphasize that the creation of surface oxygen vacancies is crucial for ORR kinetics in nano-structured cathodes. Conversely, Fe-based systems continue to perform moderately while having better chemical compatibility with electrolytes [44].

For IT-SOFC cathodes, durability remains the biggest challenge. Fe-based materials provide better phase integrity and thermal stability during long-term use [27 38 106], while Mn-based perovskites exhibit moderate redox tolerance[107]. Although Ni-based materials perform better, they experience surface segregation and oxygen loss after prolonged exposure [27 45]. When $\delta > 0.2$, Zhan,

W. et al[44] found that Ni-rich systems experience faster structural degradation. Seo, J. et al. [46] demonstrated that interface engineering and A-site deficiency improve the chemical resilience of $LaFe_{0.5}Ni_{0.5}O_3$ cathodes. For IT-SOFC operation, Mn-based systems offer a good balance between moderate conductivity and tolerable durability.

6. Electrial and Magnetic Conductivuty Correlation

Comparative examination of recent studies shows that electronic and magnetic conductivities are closely linked via the distribution of B-site valence and oxygen nonstoichiometry (δ). These factors play a significant role in influencing the transport and catalytic properties of $La_{0.7}Sr_{0.3}BO_3$ (B = Fe, Mn, Ni) materials when subjected to IT-SOFC conditions.

In Fe- and Mn-based perovskites, the charge transfer mainly happens via small-polaron hopping and double-exchange interactions among mixed-valence cations, namely Fe^{3+}/Fe^{4+} or Mn^{3+}/Mn^{4+} [15 26].This mechanism of mixed-valence exchange links spin alignment with charge mobility, resulting in magneto-transport behavior that significantly impacts the overall electronic conductivity [38]. As the substitution of Sr rises and the δ value increases, the ferromagnetic order becomes more pronounced, peaking at an optimal δ of approximately 0.15, which enhances both magnetic conductivity and electron hopping [36 48]. However, surpassing this point leads to an overabundance of oxygen vacancies that disrupt the B–O–B superexchange pathways, causing a decline in magnetic coherence and compromised overall conductivity [32].

In Ni-based perovskites, the primary mode of conduction is influenced more by band-like transport than by magnetic exchange. The overlap between delocalized Ni 3d and O 2p states enhances the electronic bandwidth, though it diminishes magnetic ordering [40]. As a result, electronic conductivity reaches its peak, but the absence of spin-coupled conduction leads to a weak magnetic response and reduced thermal stability when exposed to oxidizing environments. In contrast, Fe/Mn-rich systems exhibit a combination of spin and charge transport mechanisms, which provides them with greater redox tolerance and better resistance to distortions in the lattice[107].

The relationship between δ, B-site valence, and spin polarization establishes a three-way equilibrium among electrical, magnetic, and electrochemical characteristics[48]. Research uniformly indicates that an intermediate range of δ (0.10–0.18) along with optimized Fe/Mn ratios results in the most effective joint electronic-magnetic conductivity, which aligns with the minimal polarization resistance observed in IT-SOFC cathodes [43 108].

7. Conclusion

This review has comprehensively examined how substituting B-site cations (Fe, Mn, Ni) influences the structural, electronic, magnetic, and electrochemical characteristics of $La_{0.7}Sr_{0.3}BO_3$ perovskites used in intermediate-temperature solid oxide fuel cells (IT-SOFCs). The gathered evidence indicates that the selection of B-site cation is crucial in determining the interplay among electrical and magnetic conductivity, the occurrence of oxygen vacancies, and thermochemical stability. Systems based on Fe demonstrate remarkable structural integrity and long-term durability, although they exhibit restricted electronic movement; systems utilizing Ni exhibit excellent electronic conductivity and enhanced activity in the oxygen reduction reaction (ORR), but face challenges such as oxygen depletion and phase instability; on

the other hand, Mn-based systems provide a balanced compromise, ensuring adequate conductivity and magnetic ordering while maintaining moderate stability.

A correlation analysis has shown that the relationship between δ, B–O–B orbital overlap, and spin polarization is crucial in understanding the simultaneous development of electronic and magnetic conduction. An appropriate level of oxygen nonstoichiometry ($\delta \approx 0.10–0.18$) combined with a balanced ratio of Fe to Mn results in ideal performance, as both charge transport and ferromagnetic interactions help maintain low polarization resistance when subjected to IT-SOFC conditions. The examined literature indicates that aiming to enhance conductivity while neglecting the magnetic and structural coherence results in decreased durability, which is a significant drawback for Ni-rich systems.

In summary, the development of next-generation La-based perovskite cathodes must prioritize compositional equilibrium over extreme doping methods. Strategies involving dual substitutions at the B-site, such as Fe/Ni and Mn/Ni, along with interface engineering, have been recognized as effective approaches to improve both activity and durability. Subsequent studies should concentrate on conducting in situ magnetic and spectroscopic examinations to elucidate the interactions among spin, charge, and lattice distortions. This understanding will aid in the methodical design of cathodes capable of maintaining long-term stability while delivering consistent ORR performance at moderate temperatures.

REFERENCE

1. Nisar J, Kaur G, Giddey S, Bhargava S, Jones L. Cathode materials for intermediate temperature solid oxide fuel cells. *Fuels*. 2024;5(4):805–824.
2. Sharma P. Role of energy efficiency in energy transition: A decomposition analysis of energy use. *Solar Compass*. 2024;12:100086.
3. Zhang M, Jeerh G, Zou P, Lan R, Wang M, Wang H, Tao S. Recent development of perovskite oxide-based electrocatalysts and their applications within selected low to intermediate temperature fuel cells. *Materials Today*. 2021;49:351–377.
4. Gedik A, Lubos N, Kabelac S. Coupled transport effects in solid oxide fuel cell modeling. *Entropy*. 2022;24:224.
5. Iliev IK. Theoretical and experimental studies of combined heat and power systems with SOFCs. *Energies*. 2023;16:1898.
6. Yuan Q, Li X, Han S, Wang S, Wang M, Chen R, Kudashev S, Wei T, Chen D. Performance analysis and optimization of SOFC/GT hybrid systems: A review. *Energies*. 2024;17:1265.
7. Corigliano O, Pagnotta L, Fragiacomo P. On the technology of solid oxide fuel cell (SOFC) energy systems for stationary power generation: A review. *Sustainability*. 2022;14:15276.
8. Mehran MT, Khan MZ, Song R, Lim T, Naqvi M, Raza R, Zhu B, Hanif MB. A comprehensive review on durability improvement of solid oxide fuel cells for commercial stationary power generation systems. *Applied Energy*. 2023;352:121864.
9. Li M, Wang J, Chen Z, Qian X, Sun C, Gan D, Xiong K, Rao M, Chen C, Li X. Comprehensive review of thermal management in solid oxide fuel cells: Focus on burners, heat exchangers, and strategies. *Energies*. 2024;17:1005.
10. Ndubuisi A, Abouali S, Singh K, Thangadurai V. Recent advances, practical challenges, and perspectives of intermediate temperature solid oxide fuel cell cathodes. *Journal of Materials Chemistry A*. 2022;10:2196–2227.
11. Golkhatmi SZ, Asghar MI, Lund PD. A review on solid oxide fuel cell durability: Latest progress, mechanisms, and study tools. *Renewable and Sustainable Energy Reviews*. 2022;161:112339.

12. Niu Y. Enhancing oxygen reduction activity and structural stability of perovskite materials for SOFC cathodes. *Advanced Functional Materials*. 2021;31(14):2100034.
13. Samreen A, Ali MS, Huzaifa M, Ali N, Hassan B, Ullah F, Ali S, Arifin NA. Advancements in perovskite-based cathode materials for solid oxide fuel cells: A comprehensive review. *The Chemical Record*. 2024;24(1):e202300247.
14. Sun C, Alonso JA, Bian J. Recent advances in perovskite-type oxides for energy conversion and storage applications. *Advanced Energy Materials*. 2021;11(2):2000459.
15. Telford DM. Average and local structure of $La_{1-x}Sr_xFe_{1-\gamma}Mn_\gamma O_3{-}\delta$ oxygen-carrier materials. *Chemistry of Materials*. 2025;37(9):3471–3482.
16. Guo W, Yang Z, Dang J, Wang M. Progress and perspective in Dion–Jacobson phase 2D layered perovskite optoelectronic applications. *Nano Energy*. 2021;86:106129.
17. Cheraparambil H, Paredes MV, Scheu C, Weidenthaler C. Unraveling the evolution of dynamic active sites of catalysts during OER. *ACS Applied Materials & Interfaces*. 2024;16:21997–22006.
18. Hemberger J, Krimmel A, Kurz T, Krug von Nidda HA, Ivanov VY, Mukhin AA, Balbashov AM, Loidl A. Structural, magnetic, and electrical properties of single-crystalline $La_{1-x}Sr_xMnO_3$. *Physical Review B*. 2002;66:094410.
19. Alkhalifah MA, Howchen B, Staddon J, Celorrio V, Tiwari D, Fermin DJ. Correlating orbital composition and activity of LaMnxNi1–xO3 nanostructures toward oxygen electrocatalysis. *Journal of the American Chemical Society*. 2022;144(10):4439–4447.
20. Chiba R, Yoshimura F, Sakurai Y. An investigation of LaNi1−xFexO3 as a cathode material for solid oxide fuel cells. *Solid State Ionics*. 1999;124(3–4):281–288.
21. Ji Q, Bi L, Zhang J, Cao H. The role of oxygen vacancies of ABO3 perovskite oxides in the oxygen reduction reaction. *Energy & Environmental Science*. 2020;13(5):1408–1428.
22. Yin WJ, Wei SH, Al-Jassim MM, Yan Y. Origin of the diverse behavior of oxygen vacancies in ABO3 perovskites: A symmetry-based analysis. *Physical Review B*. 2012;85:201201.
23. Yamamoto M, Aihara T, Wachi K, Hara M, Kamata K. Perovskite oxide nanoparticles for low-temperature aerobic oxidation of isobutane to tert-butyl alcohol. *ACS Applied Materials & Interfaces*. 2024;16:62244–62253.
24. Zhu K, Shi F, Zhu X, Yang W. The roles of oxygen vacancies in electrocatalytic oxygen evolution reaction. *Nano Energy*. 2020;73:104761.
25. Li Z, Mao X, Feng D, Li M, Xu X, Luo Y, Zhuang L, Lin R, Zhu T, Liang F, Huang Z, Liu D, Yang Z, Du A, Shao Z, Zhu Z. Prediction of perovskite oxygen vacancies for oxygen electrocatalysis at different temperatures. *Nature Communications*. 2024;15:2926.
26. Pchelina DI. Structural and magnetic features of perovskite oxides $La_{1-x}Sr_xMnO_{3+\delta}$ depending on Sr content and heat treatment. *Journal of Alloys and Compounds*. 2023;938:165378.
27. ku MH, Yahia IS, Hussien MSA. Structure, magnetic, and photocatalysis of La0.7Sr0.3MO3 perovskite nanoparticles. *Environmental Science and Pollution Research*. 2023;30:61106–61122.
28. Zener C. Interaction between the d-shells in the transition metals. II. Ferromagnetic compounds of manganese with perovskite structure. *Physical Review*. 1951;82:403.
29. Dagotto E, Hotta T, Moreo A. Colossal magnetoresistant materials: The key role of phase separation. *Physics Reports*. 2001;344:1–153.
30. Sánchez-Caballero A, Zamudio-García J, Dos Santos-Gómez L, da Silva I, Pérez-Coll D, Porras-Vázquez JM, Marrero-López D. Reduced thermal expansion and improved electrochemical performance in Pr-substituted SrFeO3 as symmetrical electrode for solid oxide fuel cells. *ACS Applied Materials & Interfaces*. 2025;17(14):21380–21391.

31. Moussa F, Hennion M, Rodriguez-Carvajal J, Moudden H, Pinsard L, Revcolevschi A. Spin waves in the antiferromagnet perovskite LaMnO3. *Physical Review B*. 1996;54(21):15149–15155.
32. Kotha V, Karajagi I, Ghosh PC, Panchakarla LS. Potassium-substituted LaMnO3 as a highly active and exceptionally stable electrocatalyst toward bifunctional oxygen reduction and oxygen evolution reactions. *ACS Applied Energy Materials*. 2022.
33. Xie M, Cai C, Duan X, Xue K, Yang H, An S. Review on Fe-based double perovskite cathode materials for solid oxide fuel cells. *Energy Materials*. 2024;4(1):1–24.
34. Liu J, Jia E, Wang L, Stoerzinger KA, Zhou H, Tang CS, Yin X, He X, Bousquet E, Bowden ME, Wee ATS, Chambers SA, Du Y. Tuning the electronic structure of LaNiO3 through alloying with strontium to enhance oxygen evolution activity. *Advanced Science*. 2019;6(19):1901073.
35. Guo Q, Li X, Wei H, Liu Y, Li L, Yang X, Zhang X, Liu H, Lu Z. Sr, Fe co-doped perovskite oxides with high performance for oxygen evolution reaction. *Frontiers in Chemistry*. 2019;7:224.
36. Yang Q, Wang G, Wu H, Beshiwork BA, Tian D, Zhu S, Yang Y, Lu X, Ding Y, Ling Y, Chen Y, Lin B. A high-entropy perovskite cathode for solid oxide fuel cells. *Journal of Alloys and Compounds*. 2021;857:159633.
37. Koohfar S, Ghasemi M, Hefen T, Dimitrakopoulos G, Kim D, Pike J, Elangovan S, Gomez ED, Yildiz B. Improvement of oxygen-reduction activity and stability on a perovskite oxide surface by electrochemical potential. *Nature Communications*. 2023;14:7203.
38. Goodenough JB. Theory of the role of covalence in the perovskite-type manganites [La,M(II)]MnO_3. *Physical Review*. 1955;100:564–573.
39. Zhang S, Dou Y, Xia T, Sun L, Zhao H, Li Q. Achieving electrocatalytic activity toward oxygen reduction reaction based on Ruddlesden–Popper type cathode catalyst for solid oxide fuel cells. *Journal of Advanced Ceramics*. 2025;10(2):9221178.
40. Wang L, Adiga P, Zhao J, Samarakoon WS, Stoerzinger KA, Spurgeon SR, Matthews BE, Bowden ME, Sushko PV, Kaspar TC, Sterbinsky GE, Heald SM, Wang H, Wang LW, Wu J, Guo EJ, Qian H, Wang J, Varga T, Thevuthasan S, Feng Z, Yang W, Du Y, Chambers SA. Understanding the electronic structure evolution of epitaxial $LaNi_{1-x}Fe_xO_3$ thin films for water oxidation. *Nano Letters*. 2021;21(19):8324–8331.
41. Xue L, Li S, An S, Li N, Ma H, Li M. Preparation and properties of Fe-based double perovskite oxide as cathode material for intermediate-temperature solid oxide fuel cell. *Molecules*. 2024;29:5299.
42. Shaheen N, Chen Z, Nong Y, Su T, Yousaf M, Lu Y, Li L. Enhancing ORR catalytic activity and electrochemical investigation of $La_{1-2x}Ba_xBi_xFeO_3$ cathode for low-temperature solid oxide fuel cell. *Crystals*. 2023;13(5):822.
43. Liu J, Roddatis V, Pisarev RV, Olevano V, Alff L. Direct observation of oxygen vacancy diffusion and ordering in $La_{0.8}Sr_{0.2}MnO_{3-\delta}$ perovskite thin films. *Applied Physics Letters*. 2019;115(19):191603.
44. Zhan W, Zhou Y, Chen T, Miao G. Long-term stability of infiltrated $La_{0.8}Sr_{0.2}CoO_{3-\delta}$, $La_{0.58}Sr_{0.4}Co_{0.2}Fe_{0.8}O_{3-\delta}$ and $SmBa_{0.5}Sr_{0.5}Co_2O_{5+\delta}$ cathodes for low temperature solid oxide fuel cells. *International Journal of Hydrogen Energy*. 2015;40(46):16532-16539.
45. Jia T, Hao Y, Hao H. Sulfur-doping effects on the oxygen vacancy formation of $LaBO_3$ (B = Fe, Co and Ni) perovskites. *Physical Chemistry Chemical Physics*. 2025;27(3):1585–1592.
46. Seo J, Kim S, Jeon S, Kim S, Kim JH, Jung WC. Nanoscale interface engineering for solid oxide fuel cells using atomic layer deposition. *Nanoscale Advances*. 2022;4:1060–1073.

47. Dara M, Hassanpour M, Alshamsi HA, Baladi M, Salavati-Niasari M. Green sol–gel combustion synthesis and characterization of double perovskite Tb_2ZnMnO_6 nanoparticles and a brief study of photocatalytic activity. *RSC Advances*. 2021;11:8228–8238.
48. Tayari F, Nassar KI, Carvalho JP, Teixeira SS, Hammami I, Gavinho SR, Graça MPF, Valente MA. Sol–gel synthesis and comprehensive study of structural, electrical, and magnetic properties of $BiBaO_3$ perovskite. *Gels*. 2025;11(6):450.
49. Kaur P, Singh K. Review of perovskite-structure related cathode materials for solid oxide fuel cells. *Ceramics International*. 2020;46(5):5521–5535.
50. Beall CE, Barton JL, Liu Z. Perovskite oxide based electrodes for the oxygen reduction reaction. *ACS Catalysis*. 2021;11(18):11597–11637.
51. Sánchez Caballero A, Zamudio-García J, Dos Santos-Gómez L, da Silva I, Pérez-Coll D, Porras-Vázquez JM, Marrero-López D. Reduced thermal expansion and improved electrochemical performance in Pr-substituted $SrFeO_3$ as symmetrical electrode for solid oxide fuel cells. ACS Appl Mater Interfaces. 2025;17(14):21380–21391.
52. Raza R. Progress and prospects in cathode materials for intermediate-temperature SOFCs. Renew Sustain Energy Rev. 2024;189:113105.
53. Shen Z, Zhuang Y, Li W, Huang X, Oropeza FE, Hensen EJM, Hofmann JP, Cui M, Tadich A, Qi D, Cheng J, Li J, Zhang KHL. Increased activity in the oxygen evolution reaction by Fe^{4+}-induced hole states in perovskite $La_{1-x}Sr_xFeO_3$. J Mater Chem A. 2020;8(9):4407–4415.
54. Feng Y, Jin H, Wang S. Oxygen migration performance of $LaFeO_3$ perovskite-type oxygen carriers with Sr doping. Phys Chem Chem Phys. 2023;25:9216–9224.
55. Lu Z. Mössbauer spectroscopic analysis of $La_{1-x}Sr_xFeO_{3-\delta}$ perovskites. Phys Status Solidi B. 2023.
56. Niu Y. Enhancing oxygen reduction activity and structural stability of perovskite materials for SOFC cathodes. Adv Funct Mater. 2021;31(14):2100034.
57. Chen H, Wang T, Liu P. The role of oxygen vacancies in regulating the electrical conductivity of $La_{0.7}Sr_{0.3}MnO_3$-based cathodes for intermediate-temperature solid oxide fuel cells. J Mater Chem A. 2024;12(11):6062–6071.
58. Hoedl MF, Shapovalov V, Morgan D. Interdependence of oxygenation and hydration in mixed-conducting perovskites ($La_{1-x}Sr_xFeO_{3-\delta}$). J Phys Chem C. 2020;124(29):15856–15867.
59. Guan J, Lu L, Guo Y, Fan G. A-site doped $LaFeO_3$ perovskite for highly active O_3 catalytic decomposition. Mater Today Commun. 2024;40:109820.
60. Wu B, Xu Q, Guan W, Liu Z, Wang F, Zhang Q. A first-principles study of doping effect on enhancing ORR performance of Sr–Ni–Nb co-doped $LaFeO_3$ perovskite. Int J Hydrogen Energy. 2023;48(49):18744–18752.
61. Lim T, Lee H. Surface modification of Fe-based perovskite oxide via $Sr_{0.95}Ce_{0.05}CoO_{3-\delta}$ infiltration: A strategy for thermochemical stability. Nanomaterials. 2025;15(12):934.
62. Bai J, Niu L, Zhu Q, Zhou D, Zhu X, Wang N, Yan W, Wang J, Liang Q, Wang C. Ni-doped Fe-based perovskite to obtain multifunctional and highly efficient electrocatalytic active IT-SOFC electrode. Fuel. 2024;131334.
63. Shin Y, Doh KY, Kim SH, Lee JH, Bae H, Song SJ, Lee D. Effect of oxygen vacancies on electrical conductivity of $La_{0.5}Sr_{0.5}FeO_{3-\delta}$ from first-principles calculations. J Mater Chem A. 2020;8(9):4474–4481.
64. Triyono D, Fitria SN, Hanifah U. Dielectric analysis and electrical conduction mechanism of $La_{1-x}Bi_xFeO_3$ ceramics. RSC Adv. 2020;10(31):18482–18492.
65. Song J, Zhu S, Ning D, Bouwmeester HJM. Defect chemistry and transport properties of perovskite-type oxides $La_{1-x}Ca_xFeO_{3-\delta}$. J Mater Chem A. 2021;9(2):839–850.

66. Hartmann C, Laurencin J, Geneste G. Hole polarons in $LaFeO_3$ and $La_{1-x}Sr_xFeO_{3-\delta}$: Stability, trapping, mobility, effect of Sr concentration, and oxygen vacancies. Phys Rev B. 2023;107(2):024104.
67. Marasi M, Panunzi AP, Duranti L, Lisi N, Di Bartolomeo E. Enhancing oxygen reduction activity and structural stability of $La_{0.6}Sr_{0.4}FeO_{3-\delta}$ by 1 mol% Pt and Ru B-site doping for application in all-perovskite IT-SOFCs. ACS Appl Energy Mater. 2022;5(3):2882–2892.
68. Panunzi AP, Duranti L, Luisetto I, Lisi N, Marelli M, Di Bartolomeo E. Triggering electrode multi-catalytic activity for reversible symmetric solid oxide cells by Pt-doping lanthanum strontium ferrite. Chem Eng J. 2023;471:144448.
69. Lin W, Li Y, Singh M, Zhao H, Yang R, Su PC, Fan L. Electronic engineering and oxygen vacancy modification of $La_{0.6}Sr_{0.4}FeO_{3-\delta}$ perovskite oxide by low-electronegativity sodium substitution for efficient CO_2/CO-fueled reversible solid oxide cells. Green Chem. 2024;26(6):3505–3516.
70. Xue LM, Li SB, An SL, Li N, Ma HP, Li MX. Fe-based double perovskite with Zn doping for enhanced electrochemical performance as intermediate-temperature solid oxide fuel cell cathode material. RSC Adv. 2023;13:30606–30614.
71. Jacobs R, Mayeshiba T, Booske J, Morgan D. Material Discovery and Design Principles for Stable, High Activity Perovskite Cathodes for Solid Oxide Fuel Cells. *Advanced Energy Materials*. 2018;8(11):1702708.
72. Li N, Sun L, Li Q, Xia T, Huo L, Zhao H. Novel and high-performance (La,Sr)MnO_3 based composite cathodes for intermediate-temperature solid oxide fuel cells. *Journal of the European Ceramic Society*. 2023;43:5279–5287.
73. Wang W, Liu W, Kamiko M, Yagi S. Enhanced catalytic activity of perovskite $La_{1-x}Sr_xMnO_{3+\delta}$ for the oxygen reduction reaction. *New Journal of Chemistry*. 2022;46:13082–13088.
74. Bhowmick S, Dhankhar A, Sahu TK, Jena R, Gogoi D, Peela NR, Ardo S, Qureshi M. Low Overpotential and Stable Electrocatalytic Oxygen Evolution Reaction Utilizing Doped Perovskite Oxide, $La_{0.7}Sr_{0.3}MnO_3$, Modified by Cobalt Phosphate. *ACS Applied Energy Materials*. 2020;3(2):1279–1285.
75. Pham TL, Yu JH, Lee JS. Conductivity Transitions of $La_{0.7}Sr_{0.3}MnO_{3+\delta}$ and $La_{0.6}Sr_{0.4}Co_{0.2}Fe_{0.8}O_{3-\delta}$ in $Ce_{0.9}Gd_{0.1}O_2$-δ Matrix for Dual-Phase Oxygen Transport Membranes. *Crystals*. 2021;11(6):712.
76. Shan, F, Chen T, Ye L, Xie K. Ni–Doped $Pr_{0.7}Ba_{0.3}MnO_{3-\delta}$ Cathodes for Enhancing Electrolysis of CO_2 in Solid Oxide Electrolytic Cell. *Molecules*. 2024;29(18):4492.
77. Martinelli H, Lamas DG, Leyva AG, Sacanell J. Influence of particle size and agglomeration in solid oxide fuel cell cathodes using manganite nanoparticles. *Materials Research Express*. 2018;5(7):075013.
78. Xue Y, Huang H, Miao H, Sun S, Wang Q, Li S, Liu Z. One-pot synthesis of $La_{0.7}Sr_{0.3}MnO_3$ supported on flower-like CeO_2 as electrocatalyst for oxygen reduction reaction in aluminum-air batteries. *Journal of Power Sources*. 2017;358:50–60.
79. Xue Y, Miao H, Li B, Sun S, Wang Q, Li S, Chen L, Liu Z. Promoting effects of $Ce_{0.75}Zr_{0.25}O_2$ on the $La_{0.7}Sr_{0.3}MnO_3$ electrocatalyst for the oxygen reduction reaction in metal–air batteries. *Journal of Materials Chemistry A*. 2017;5(8):6411–6415.
80. Sun L, Sun T, Li X, Wang Y. $La_{0.7}Sr_{0.3}MnO_3$ Perovskites for Oxygen Reduction in Zn–Air Batteries: Enhanced by *In Situ* Glucose Regulation. *ACS Applied Materials and Interfaces*. 2025; 17(5):77716-7727.
81. Xiaoxiong L, Wang Y, Youngcun L, Liang Y. Durable bifunctional electrocatalyst for cathode of zinc-air battery: surface pre-reconstruction of $La_{0.7}Sr_{0.3}MnO_3$ perovskite by iron ions. *Journal of*

Alloys and Compounds. 2024;976:173398.

82. Shi W, ZhSHang J, Yu B, Zheng J, Wang M, Li Z, et al. Improved conduction and orbital polarization in ultrathin $LaNiO_3$ sublayer by modulating octahedron rotation in $LaNiO_3/CaTiO_3$ superlattices. *Nature Communications*. 2024;15:9931
83. Adachi Y, Hatada N, Kato M, Hirota K, Uda T. Experimental validation of high electrical conductivity in Ni-rich $LaNi_{1-x}Fe_xO_3$ solid solutions ($x \leq 0.4$) in high-temperature oxidizing atmospheres. *Materials Advances*. 2021;2:3257–3263.
84. Yao D, Wang W, Yu J, You Y. Substrate effect on the structural and electrical properties of $LaNiO_3$ thin films. *Journal of Wuhan University of Technology – Materials Science Edition*. 2022;37:559–563.
85. Cao P, Tang P, Bekheet MF, Du H, Yang L, Haug L, et al. Atomic-scale insights into nickel exsolution on $LaNiO_3$ catalysts via in situ electron microscopy. *The Journal of Physical Chemistry C*. 2022;126(1):786–796.
86. Zhu Z, Song Q, Xia B, Jiang L, Duan J, Chen S. Perovskite catalysts for oxygen evolution and reduction reactions in zinc-air batteries. *Catalysts*. 2022;12(12):1490.
87. Yuan R, Xu W, Pan L, Li R, Xiao C, Qiao X. Ni-doped $La_{0.6}Sr_{0.4}CoO_3$ perovskite as an efficient electrocatalyst for oxygen reduction and evolution reactions in alkaline media. *Catalysts*. 2023;13(10):1366.
88. Nandikes G, Gouse Peera S, Singh L. Perovskite-based nanocomposite electrocatalysts as an alternative to platinum ORR catalyst in microbial fuel cell cathodes. *Energies*. 2022;15(1):272
89. Li Q, Zhang D, Wu J, Dai S, Liu H, Lu M, et al. Cation-deficient perovskites greatly enhance the electrocatalytic activity for oxygen reduction reaction. *Advanced Materials*. 2024;36(7):2309266.
90. Rudolph B, Tsiotsias AI, Ehrhardt B, Dolcet P, Gross S, Haas S, et al. Nanoparticle exsolution from nanoporous perovskites for highly active and stable catalysts. *Advanced Science*. 2023;10(6):e2205890.
91. Zhang Bo-Wen, Zhu Meng-Nan, Gao Min-Rui, Xi Xiuan, Duan Nanqi, Chen Zhou, Feng Ren-Fei, Zeng Hongbo, Luo Jing-Li. Boosting the stability of perovskites with exsolved nanoparticles by B-site supplement mechanism. *Nature Communications*. 2022;13:4618.
92. Tarutin AP, Kasyanova AV, Vdovin GK, Lyagaeva JG, Medvedev DA. Nickel-containing perovskites $PrNi_{0.4}Fe_{0.6}O_{3-\delta}$ and $PrNi_{0.4}Co_{0.6}O_{3-\delta}$ as potential electrodes for protonic ceramic electrochemical cells. *Materials*. 2022;15:2166.
93. She S, Zhao Y, Park J, Li Z, Cho J. Improved conduction and orbital polarization in ultrathin $LaNiO_3$ sublayer by modulating octahedron rotation in $LaNiO_3/CaTiO_3$ superlattices. *Advanced Functional Materials*. 2021;31(51):21011091.
94. Liu H, Wei L, Zheng H, Tang K. Fe–Ni co-doping strategy in perovskite for developing an efficient oxygen evolution electrocatalyst. *Chinese Journal of Chemical Physics*. 2023;36(6):764–772.
95. Muñoz HJ, Korili SA, Gil A. Recent advances in the application of Ni-perovskite-based catalysts for the dry reforming of methane. *Catalysis Reviews*. 2024.
96. Weber ML, Jennings D, Fearn S, Cavallaro A, Prochazka M, Gutsche A, et al. Thermal stability and coalescence dynamics of exsolved Ni nanoparticles on acceptor- and donor-doped perovskite oxide surfaces. *Nature Communications*. 2024;15(1):9724.
97. Xue X, Li B. Recent advances in nanostructured perovskite oxide synthesis and application for electrocatalysis. *Nanomaterials*. 2025;15(6):472.
98. Chowdhury TA, Bin Zafar MA, Sajjad-Ul Islam M, Shahinuzzaman M, Islam MA, Khandaker MU. Stability of perovskite solar cells: Issues and prospects. *RSC Advances*. 2023;13(3):1787–1810.
99. Kersell H, Weber ML, Falling L, Lu Q, Baeumer C, Shirato N, et al. Evolution of surface and

subsurface morphology and chemical state of exsolved Ni nanoparticles. *Faraday Discussions*. 2022;236:141–156.

100. Fossdal, A., Menon, M., Waernhus, I. and Wiik, K. Crystal structure and thermal expansion of $La_{1-x}Sr_xFeO_{3-\delta}$ materials. *Journal of the American Ceramic Society.* 2004;87(10):1952–1958.
101. Che, Q., van den Bosch, I. C. G., Le, P. T. P., Lazemi, M., van der Minne, E., Abrikhlozer, Y., Zunnenkamp, M., Peerlings, M. L. J., Safonova, O. V., Nachtegaal, M., Koster, G., Baumer, C., de Jongh, P., and de Groot, F. M. F. In situ X-ray absorption spectroscopy of $LaFeO_3$ and $LaFeO_3/LaNiO_3$ thin films in the electrocatalytic oxygen evolution reaction. *The Journal of Physical Chemistry C*. 2024;128(13):5515–5523.
102. Freeland, J. W., van Veenendaal, M., and Chakhalian, J. Evolution of electronic structure across the rare-earth $RNiO_3$ series. *Journal of Electron Spectroscopy and Related Phenomena*. 2016;208:56–62.
103. Urushibara, A., Moritomo, Y., Arima, T., Asamitsu, A., Kido, G. and Tokura, Y. Insulator–metal transition and giant magnetoresistance in $La_{1-x}Sr_xMnO_3$. *Physical Review B.* 1995;51(20):14103–14109.
104. Tai, L. W., Nasrallah, M. M., Anderson, H. U., Sparlin, D. M., and Sehlin, S. R. Structure and electrical properties of $La_{1-x}Sr_xCo_{1-\gamma}Fe_\gamma O_3$. Part 1. The system $La_{0.8}Sr_{0.2}Co_{1-\gamma}Fe_\gamma O_3$. *Solid State Ionics*. 1995;76(3–4):259–271.
105. García-Muñoz, J. L., Rodríguez-Carvajal, J., Lacorre, P., and Torrance, J. B. Neutron-diffraction study of $RNiO_3$ (R = La, Pr, Nd, Sm): Electronically induced structural changes across the metal–insulator transition. *Physical Review B.* 1992;46(8):4414–4425.
106. Stoerzinger, K. A., Choi, W. S., Jeen, H., Lee, H. N., and Shao-Horn, Y. Role of strain and surface reconstruction in oxygen electrocatalysis on perovskite thin films. *Nature Chemistry*. 2015;7(4):309–315.
107. Adler,S.B. Factors governing oxygen reduction in solid oxide fuel cell cathodes. *Journal of the Electrochemical Society*. 2004;151(3):A323–A331.
108. Suntivich, J., May, K. J., Gasteiger, H. A., Goodenough, J. B., and Shao-Horn, Y. A perovskite oxide optimized for oxygen evolution catalysis from molecular orbital principles. *Science*. 2011;334(6061):1383–1385.